25th ABCM International Congress of Mechanical Engineering
October 20-25, 2019, Uberlândia, MG, Brazil

NUMERICAL MODELLING OF HELICAL CABLES USING BEAM-BASED METAELEMENTS

Eduardo Antonio Wink de Menezes
UFRGS, PROMEC, Rua Sarmento Leite, 425
eduardo.menezes@ufrgs.br
Sandro Campos Amico
UFRGS, PROMEC, Rua Sarmento Leite, 425
amico@ufrgs.br
Rogério José Marczak
UFRGS, PROMEC, Rua Sarmento Leite, 425
rato@mecanica.ufrgs.br

Abstract. *Cables and wire ropes are structural components designed for high axial stresses and relatively low torsional and flexural stress, where their high flexibility under bending is achieved through the helical construction of the wires surrounding the cable core. Typical applications include cable-stayed bridges, mooring lines in offshore structures, cranes, mine hoisting, lifts, among others. In comparison with steel cables, composite cables show low degradation under harsh environments, outstanding fatigue life, and higher specific Young's modulus and strength especially due to their lightweight. These features have enabled offshore platforms to be installed in deeper water and the increase in cable-stayed bridge span. Given the complex geometry of helical cables, analytical models for predicting their mechanical behavior include many assumptions and simplifications. As for numerical models, although they can reproduce the cable behavior with reasonable accuracy, they can only simulate a limited length, restricting their application in many practical cases. In order to overcome that, a finite element model was developed in which a new beam element was designed aiming at incorporating the features of a cable modeled through solid elements. The proposed element was able to combine the accuracy of numerical models and the easy implementation of analytical solutions.*

Keywords: *helical cable, finite element method, beam element*

1. INTRODUCTION

For many years, the use of composite materials was limited to aerospace and military applications due to their high cost coupled with the difficulties related to the design of structures (e.g. anisotropy, failure, interface phenomena, etc.). In the 1990s, as their cost reduced, they became a feasible and attractive solution for many different sectors (Adanur et al., 2011), including cables based on epoxy resin reinforced with carbon fibers. Relative to steel cables, their advantages include corrosion resistance, low thermal expansion coefficient, lightweight, and higher fatigue life, specific Young modulus and mechanical strength (Xie and Shen, 2014). On the other hand, they require complex anchorage systems and present lower shear strength and thermal stability (Cai and Aref, 2015). Despite its high cost per weight, it has been shown that the final cost can be significantly reduced by substituting steel for CFRP (Carbon Fiber Reinforced Polymer) cables due to the lower amount of material required (Liu et al., 2016). This substitution may also considerably reduce maintenance costs and increase maximum span in cable-stayed bridges (Meier, 2012).

Regarding the offshore industry, the remarkable corrosion resistance of the cable allows good mechanical properties even after seawater aging for 7000 h (Ali et al., 2015). Due to their lightweight, they also display high natural frequencies even in ultra-deep waters (Odru and Geffroy, 2002) and have the potential to make TLPs (Tension Leg Platforms) feasible in water depths of up to 3000 m (Botker and Johannessen, 2002).

Modeling helical cables is not an easy task. Several attempts were made over the years, aiming to accurately reproduce their mechanical behavior through analytical models. None of them, however, could incorporate all the essential features, and common assumptions include frictionless/rough contact conditions, neglection of wires contraction and linear elastic isotropic materials. Also, they are available for limited loading and boundary conditions (Cardou and Jolicoeur, 1997). Another critical limitation that makes analytical models to significantly deviate from the real behavior is the relative slippage between wires and core, as highlighted by Ghoreishi et al. (2007). On the other hand, numerical models elaborated through FEM (Finite Element Method) can accurately match experimental results, even for CFRP cables under different loading conditions (Menezes et al., 2017) (Luz et al., 2018), but may require high computational time to simulate the cable, and all its contact pairs (wire/wire, wire/core), even for a short cable with simple geometry.

This paper aims to design a new beam element, herewith referred as metaelement, able to simulate helical cables and carrying the same information of cables modeled through solid elements, focusing on low computational time, while also keeping relatively good accuracy.

2. METHODOLOGY

2.1 Analytical models

Ghoreishi et al. (2007) evaluated the stiffness matrix **K** of 1×7 cables for different helix angles considering two degrees of freedom, longitudinal displacement and rotation around the longitudinal axis (*x*). Eight different analytical models were tested and the best results relative to the numerical solution were the ones that considered the stiffness matrix as non-symmetric. The relation between force and displacement is given by:

$$\begin{bmatrix} F_x \\ M_x \end{bmatrix} = \begin{bmatrix} K_{11} & K_{12} \\ K_{21} & K_{22} \end{bmatrix} \begin{bmatrix} u_x \\ \theta_x \end{bmatrix} \tag{1}$$

where F and M are force and moment, respectively, u and θ are displacement and rotation, respectively, and the stiffness coefficients K_{ij} are shown below

$$K_{11} = \frac{E_c A_c + N E_w A_w \cos(\beta)\left[1-(1+\nu)\eta_1 \sin^2(\beta)\right]}{L}$$

$$K_{12} = \frac{N E_w A_w (R_c + R_w)\eta_1 \cos^2(\beta)\sin(\beta)}{L}$$

$$K_{21} = \frac{N}{L}\left[E_w A_w (R_c + R_w)\sin(\beta) - \frac{E_w I_w}{(R_c + R_w)}\sin(\beta)\left(1-\eta_4\cos^4(\beta)+(1+\nu)\left(\eta_2 - 1 + \eta_4\cos^4(\beta)\right)\right)\right]$$

$$K_{22} = \frac{G_c J_c + N E_w I_w \eta_2 \cos(\beta)}{L}$$

$$\eta_1 = (1-\eta_3)\left[1-\frac{1}{4}\left(\frac{R_w}{(R_c+R_w)}\right)^2\left(1+\eta_4\cos(2\beta)\right)\sin^2(\beta)\right]$$

$$\eta_2 = (1-\eta_3)\left[4\left(\frac{(R_c+R_w)}{R_w}\right)^2\sin^2(\beta)+1-\sin^4(\beta)-\eta_4\cos^4(\beta)\cos(2\beta)\right]$$

$$\eta_3 = \nu\left[\frac{R_w}{(R_c+R_w)}\right]\sin^2(\beta)$$

$$\eta_4 = \frac{\nu}{1+\nu} \tag{2}$$

where E, G, and ν are the Young modulus', shear modulus' and Poisson ratio of the material, respectively; R, A, I, and J are the radius, area, area moment of inertia and polar moment of inertia, with subscripts w and c denoting wire and core, respectively; N is the number of external wires (6), L is the cable length, and β is the lay angle (complementary to the helix angle).

A model for pure bending was also proposed by Costello and reported below:

$$M_z = \frac{\pi E}{2L}\theta_z\left[\frac{2N\sin(\beta)R_w^4}{2+\nu\cos^2(\beta)} + R_c^4\right] \tag{3}$$

2.2 FE numerical model with solid elements

The studied cable has a 1×7 construction (six wires surrounding the core), where core and wires have the same diameter. Normal and tangential contact (penalty formulation) were considered, with a CFRP friction coefficient of 0.65 (Schön, 2004), and a 0.01 mm gap was defined between wires to avoid early penetration. To minimize computational

time, node-to-surface formulation was applied since contact pressures are of minor importance here. The material properties for carbon fiber T800 and epoxy resin MY750 were obtained from Kaddour and Hinton (2004), and the micromechanical Chamis model (Chamis, 1989) was applied to evaluate the CFRP homogenized properties considering a fiber volume fraction of 76% (see Tab. 1), where subscript 1 denotes fiber direction, while 2 and 3 are the directions orthogonal to 1. The material is considered transversally isotropic, and a local coordinate system was used to accomodate the variation in properties with the direction as the wires twist around the cable core. The chosen element is C3D8R, an eight-node hexahedral element, with one single integration point and hourglass control (Abaqus, 2013), with three degrees of freedom (translations in *x*, *y* and *z*).

Table 1. Properties of the resin matrix, the fiber, and the final composite considered in this work.

	Epoxy MY750	Carbon T800	Homogeneized composite
E_1 (MPa)	3350	234500	180000
$E_2 = E_3$ (MPa)	3350	14120	10060
$\nu_{12} = \nu_{13}$	0.350	0.246	0.271
ν_{23}	0.350	0.100	0.195
$G_{12} = G_{13}$ (MPa)	1240	14700	6217
G_{23} (MPa)	1240	6418	4209
ρ (kg/m³)	1274	1800	1676

The geometric characteristis used in the models were L = 200 mm, $R_w = R_c$ = 1.5 mm and α = 72°. Stiffness coefficients were directly evaluated through the relation shown below, assuming linear elastic behavior. The coefficient is considered to be equivalent to the generalized force applied at node *i* to produce a unity displacement at *j*, with all the other displacements being equal to zero (Tauchert, 1974).

$$K_{ij} = \frac{\partial F_i}{\partial u_j} \tag{4}$$

The required simulations to evaluate all stiffness coefficients are illustrated in Fig. 1. Since for this cable $I_y = I_z$ (valid along the length), the cases reported in Fig. 1(b) and Fig. 1(c) dismiss extra cases for deflection in *z* and rotation around *y*. The left end was clamped in all four cases, while the right end has only one degree of freedom in each case, being longitudinal displacement, transverse displacement, rotation around *z* axis, and rotation around *x* axis for the cases reported in Fig. 1(a), Fig. 1(b), Fig. 1(c) and Fig. 1(d), respectively. From now on these loading conditions are referred as *Case 1* (Fig. 1(a)), *Case 2* (Fig. 1(b)), *Case 3* (Fig. 1(c)) and *Case 4* (Fig. 1(d)).

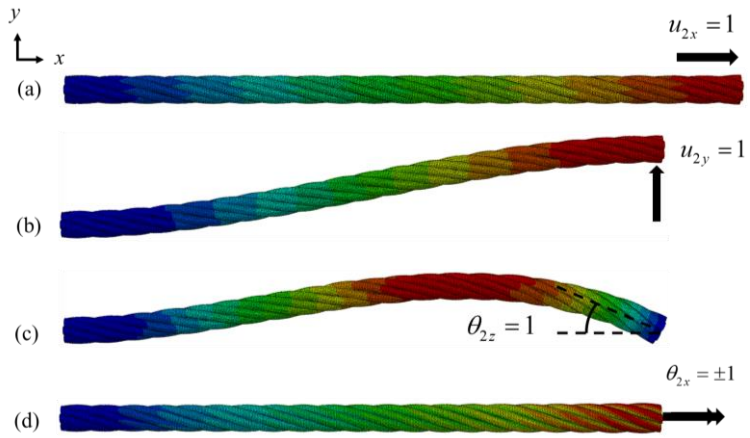

Figure 1. Simulations required to evaluate stiffness coefficients, including the application of (a) longitudinal displacement (*Case 1*), (b) vertical displacement (*Case 2*), rotation around (c) *z* and (d) *x*-axes (*Cases 3 and 4*).

2.3 FE numerical model with beam elements

To create a beam-based metaelement that accurately reproduces the results obtained through the solid element, one must investigate the influence of material and geometric parameters in the cable stiffness matrix **K**. According to

Menezes et al. (2017), except for the longitudinal Young modulus (E_1) and in-plane shear modulus (G_{12}) (from now on referred just as E and G, respectively), the other engineering constants have a negligible influence on **K**. The helix angle, however, has a complex influence in all stiffness terms (Menezes et al., 2017) (Ghoereishi et al., 2007) (Chen et al., 2017). The friction coefficient is also reported to have a small effect (Menezes et al., 2017), (Jiang and Warby, 2008). However, transition from the no-friction to the no-slippage condition may produce significant differences (Chen et al., 2017), (Jolicoeur and Cardou, 1996). Therefore, the parameters to be incorporated in the metaelement stiffness matrix are the engineering constants E and G, wire diameter (D), cable length (L) and helix angle (α).

Firstly, a sensitive analysis was performed to determine the influence of each of the above mentioned parameters in each term of **K** for the 1×7 cable modeled with solid elements. This procedure is required for the next step, which consists in elaborating a factorial design to adjust **K** to enable a reasonable prediction of the required design level f for each parameter. A series of functions φ (E, G, D, L, α) are then incorporated in the classical Euler-Bernoulli stiffness matrix with two nodes and six degrees of freedom (DOF) per node (i.e. three displacements and three rotations), as depicted in Eq. (5).

$$\mathbf{K} = \begin{bmatrix}
\varphi_1\frac{EA}{L} & 0 & 0 & \varphi_5 & 0 & 0 & -\varphi_1\frac{EA}{L} & 0 & 0 & -\varphi_5 & 0 & 0 \\
0 & \varphi_2\frac{12EI}{L^3} & 0 & 0 & 0 & \varphi_2\frac{6EI}{L^2} & 0 & -\varphi_2\frac{12EI}{L^3} & 0 & 0 & 0 & \varphi_2\frac{6EI}{L^2} \\
0 & 0 & \varphi_2\frac{12EI}{L^3} & 0 & -\varphi_2\frac{6EI}{L^2} & 0 & 0 & 0 & -\varphi_2\frac{12EI}{L^3} & 0 & -\varphi_2\frac{6EI}{L^2} & 0 \\
\varphi_4 & 0 & 0 & \varphi_3\frac{GJ}{L} & 0 & 0 & -\varphi_4 & 0 & 0 & -\varphi_3\frac{GJ}{L} & 0 & 0 \\
0 & 0 & -\varphi_2\frac{6EI}{L^2} & 0 & \varphi_2\frac{4EI}{L} & 0 & 0 & 0 & \varphi_2\frac{6EI}{L^2} & 0 & \varphi_2\frac{2EI}{L} & 0 \\
0 & \varphi_2\frac{6EI}{L^2} & 0 & 0 & 0 & \varphi_2\frac{4EI}{L} & 0 & -\varphi_2\frac{6EI}{L^2} & 0 & 0 & 0 & \varphi_2\frac{2EI}{L} \\
-\varphi_1\frac{EA}{L} & 0 & 0 & -\varphi_5 & 0 & 0 & \varphi_1\frac{EA}{L} & 0 & 0 & \varphi_5 & 0 & 0 \\
0 & -\varphi_2\frac{12EI}{L^3} & 0 & 0 & 0 & -\varphi_2\frac{6EI}{L^2} & 0 & \varphi_2\frac{12EI}{L^3} & 0 & 0 & 0 & -\varphi_2\frac{6EI}{L^2} \\
0 & 0 & -\varphi_2\frac{12EI}{L^3} & 0 & \varphi_2\frac{6EI}{L^2} & 0 & 0 & 0 & \varphi_2\frac{12EI}{L^3} & 0 & \varphi_2\frac{6EI}{L^2} & 0 \\
-\varphi_4 & 0 & 0 & -\varphi_3\frac{GJ}{L} & 0 & 0 & \varphi_4 & 0 & 0 & \varphi_3\frac{GJ}{L} & 0 & 0 \\
0 & 0 & -\varphi_2\frac{6EI}{L^2} & 0 & \varphi_2\frac{2EI}{L} & 0 & 0 & 0 & \varphi_2\frac{6EI}{L^2} & 0 & \varphi_2\frac{4EI}{L} & 0 \\
0 & \varphi_2\frac{6EI}{L^2} & 0 & 0 & 0 & \varphi_2\frac{2EI}{L} & 0 & -\varphi_2\frac{6EI}{L^2} & 0 & 0 & 0 & \varphi_2\frac{4EI}{L}
\end{bmatrix} \tag{5}$$

The coefficients of φ were computed through non-linear regression, and the finite difference method was applied to maximize the coefficient of determination (R^2) along the iteration process (Matlab, 2012). It is interesting to note that the new **K** matrix is no longer symmetric ($\varphi_4 \neq \varphi_5$) since coupling between axial tension and axial torsion (N-T) and from axial torsion and axial tension coupling (T-N) are expected to differ for cables. An unsymmetrical matrix was adopted in many analytical solutions found in the literature (Ghoereishi et al., 2007), including the above-mentioned Costello's model. The procedure to obtain **K** is summarized in Figure 2. In the stiffness plots shown in the results section, the nomenclature adopted for stiffness follows the expressions of the original Euler-Bernoulli beam element, except for the coupling.

3. RESULTS

For the longitudinal Young modulus E, the sensitivity analysis was performed between 90,000 MPa and 270,000 MPa, achieving a coefficient of determination above 0.99 in all terms of **K** for a linear fit. Therefore, a factorial level of 2 was applied to account for the E contribution. This parameter is also affected by the torsional stiffness and the coupling stiffness between torsion and tension (T-N), which is in agreement with the predictions of Costello shown in Eq. (2). This influence is illustrated in Figure 3, evaluated under *Case 4* loading condition.

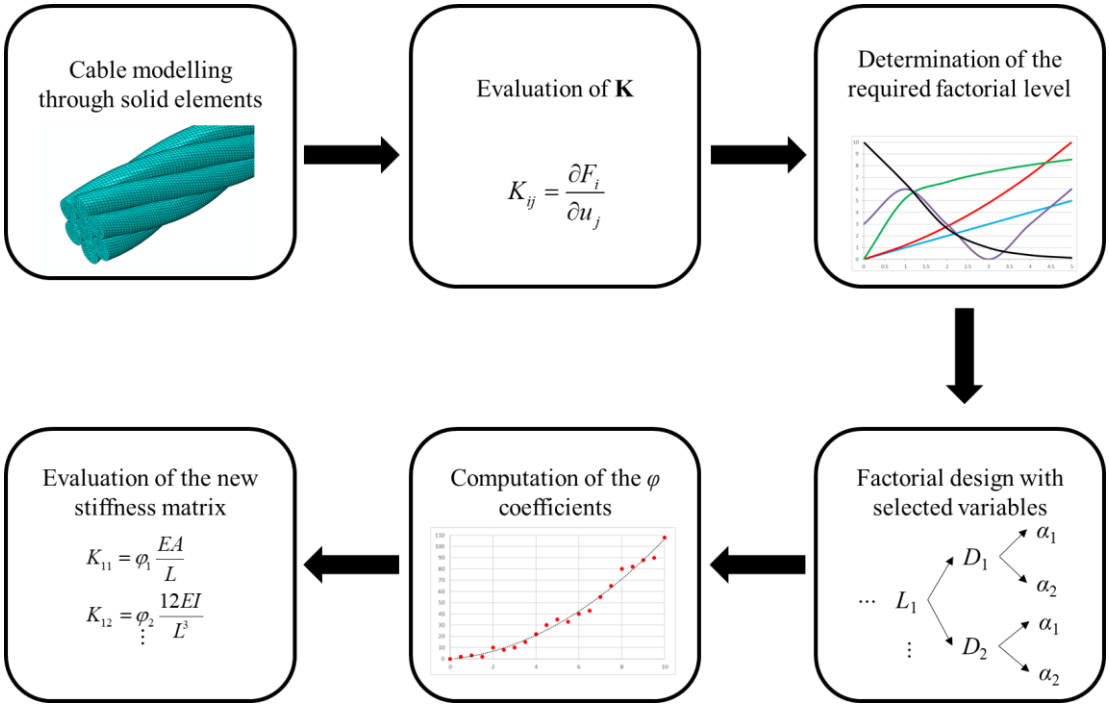

Figure 2 – Summary of the procedure to determine the metaelement stiffness matrix **K**.

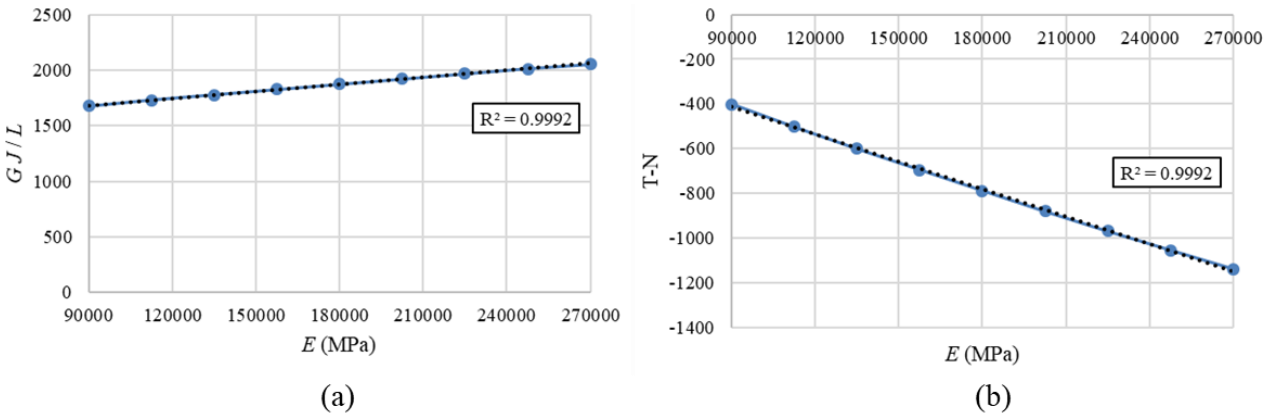

Figure 3 – Influence of *E* on torsional stiffness (a) and on coupling between torsion and tensile stiffness (b), and the respective R^2 for linear fitting.

Regarding the shear modulus *G*, its influence on the tensile and bending terms is negligible if high values are considered, such as those for metals (~70,000 MPa). However, for low values, it has a significant influence on all terms, being logarithm for the terms obtained in *Cases 1* (illustrated in Figure 4), *2 and 3*, and linear for *Case 4*. Hence, $f = 4$ was adopted for *Cases 1*, *2 and 3*, and $f = 3$ for *Case 4*. For this parameter, the R^2 obtained was around 0.95. Considering the relation between **K** and *L* presented in Eq. (5) ($1/L$, $1/L^2$, $1/L^3$), a linear fit yielded an $R^2 > 0.99$ for all cases in the 100-300 mm range. In the present study, at a small displacement range, clockwise and counterclockwise rotations yielded the same results for the boundary conditions of *Case 4*. Respecting the relation between **K** and *D* (which can be a function of *A*, *I* and *J*) in Eq. (5), an R^2 superior to 0.99 was again found, where the diameter of all wires was simultaneously changed, aiming to produce a variation of -50% and +50% on cable area. Therefore, $f = 2$ for both *L* and *D*.

The analyzed range of helix angle was 62°-82°, since values out if these bounds are unusual. The behavior was non-linear for all terms. Hence, a factorial level of 3 was adopted, except for the N-T term, for which an inflection point was observed (shown in Figure 5(a)), and $f = 5$ was chosen. It is interesting to notice that, as the helix angle increases, the coupling stiffnesses approaches zero, as can be seen in Figure 5.

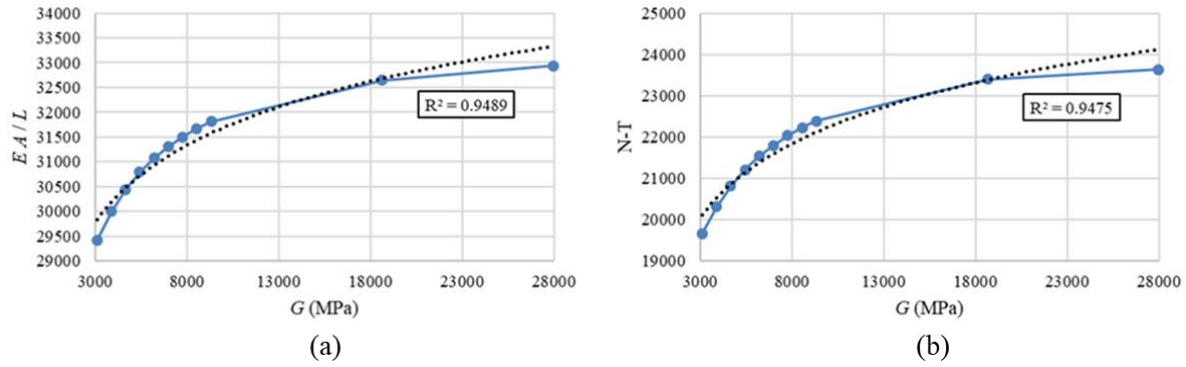

Figure 4 – Influence of G on tensile stiffness (a) and on coupling between tensile and torsional stiffness (b), with the respective R^2 for fitting.

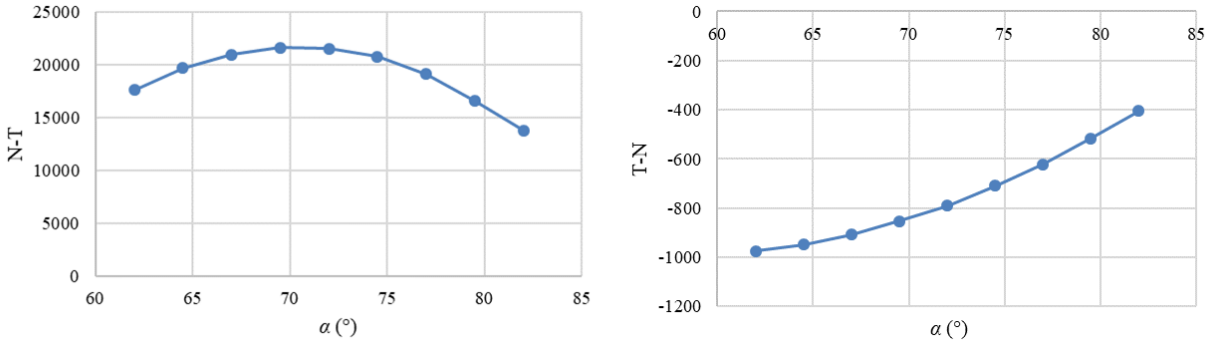

Figure 5 – (a) N-T and (b) T-N stiffnesses as a function of the helix angle.

After performing the factorial design with all possible combinations and considering the factorial levels found, yielding a total of 424 simulations, the φ coefficients could be evaluated. The applied functions accounted for the contribution of core and wires by splitting φ into a parcel independent and a parcel dependent on the helix angle. Trigonometric functions were adopted to account for α aiming to reproduce situations where it should result in clear minimax values. The final functions are shown below, along with the coefficients obtained through non-linear regression. The R^2 values were greater than 0.99, except for N-T and T-N, where 0.94 and 0.96, respectively, were obtained. The metalement stiffness matrix could then be evaluated by substituting φ into Eq. (5) and implementing it in a commercial FEM software (Abaqus, 2013).

$$
\begin{aligned}
\varphi_1 &= -3.7065 - 0.0055\ln(G)\cos(\alpha) + 4.6363\sin(\alpha) \\
\varphi_2 &= 0.2808 + 0.03092\ln(G)\cos(\alpha) - 0.1301\sin(\alpha) - 0.5130\cos(\alpha) \\
\varphi_3 &= -0.2925 + 0.0051\frac{E}{G}\cos(\alpha) + 0.4072\sin(\alpha) \\
\varphi_4 &= \frac{EA}{L}\cos(\alpha)\left[1.1181 + 0.1208\ln(G) + 1.1286\sin(\alpha) - 5.1256\cos(\alpha)\right] \\
\varphi_5 &= \cos(\alpha)\frac{J}{L}\left[0.0032G + 0.0072E - 0.0131E\sin(\alpha)\right]
\end{aligned}
\tag{6}
$$

A comparison between the stiffnesses values obtained for *Case 1* and *Case 4* for different helix angles using Costello's model, FEM model with 3D elements and FEM model with the proposed metaelement are reported in Figure 6 and Figure 7, respectively. For *Case 1*, the metaelement was able to accurately reproduce solid elements results throughout the helix angle range, yielding deviations around 5% for tensile stiffness and 8% for N-T coupling, Costello's model significantly overestimated stiffnesses values for $\alpha < 72°$. Relative to *Case 4*, the metaelement predicted with reasonable accuracy the torsional stiffness and T-N coupling, with average deviations of 5% and 20%, respectively, while Costello's model estimates were in a different order of magnitude for both of them.

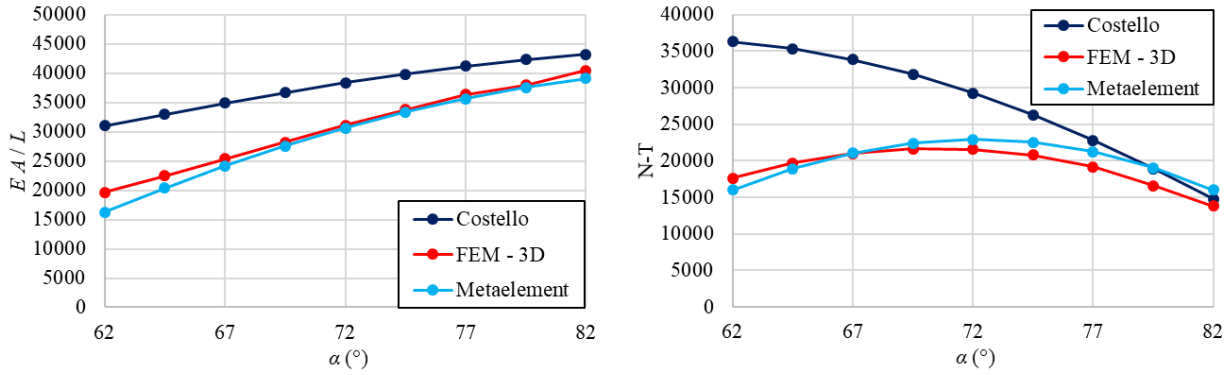

Figure 6 – Comparison between tensile stiffness and N-T coupling estimates from Costello's model, FEM model with solid elements and FEM model with metaelements for *Case 1*.

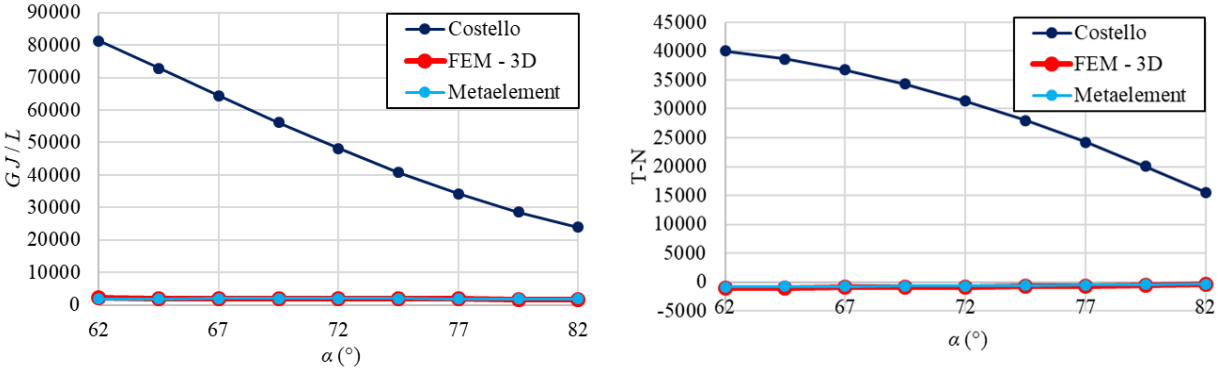

Figure 7 - Comparison between torsion stiffness and T-N coupling estimates from Costello's model, FEM model with solid elements and FEM model with metaelements for *Case 4*.

A pure bending condition was also studied, where two opposite bending moments were applied at the cable ends, in order to compare analytical (Eq. (3)) and numerical predictions, and the results are shown in Figure 8. Once again, the analytical model shows a clear trend in overestimating stiffness for low helix angles (at α = 72°, the deviation relative to the FEM model with solid elements reaches 37%). As occurred for tensile stiffness, the deviation observed in the metalement bending stiffness slightly increased for low helix angle, from less than 1% at α = 82° to 10% at α = 62°.

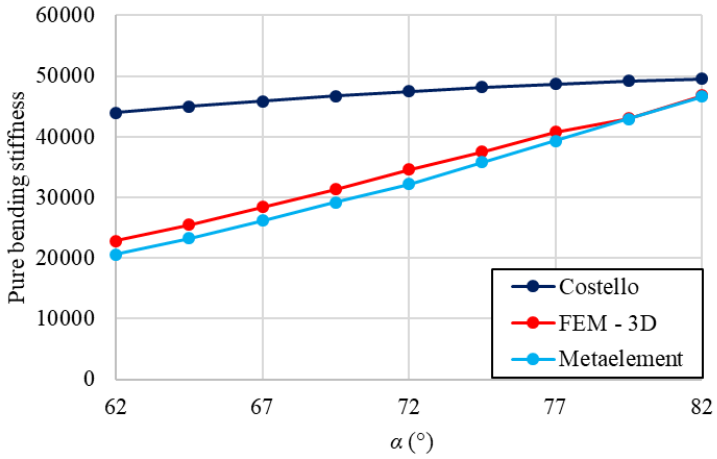

Figure 8 - Comparison between pure bending stiffness estimates from Costello's model, FEM model with solid elements and FEM model with metaelements.

4. CONCLUSIONS

This work applied the Finite Element Method to develop a metaelement, elaborated from Euler-Bernoulli beam element, able to simulate composite cables. A first study was carried out with solid elements, previously validated through experimental tests, in order to investigate characteristics of interest for helical cables and to accurately incorporate them into a metaelement.

A 1×7 cable was modelled in a FEM platform with solid elements, where a sensitivity analysis was conducted to identify the most relevant parameters in the analysis. The influence of longitudinal Young modulus, in-plane shear modulus, wires diameter, cable length and helix angle, in all terms of the cable stiffness matrix **K**, including the tension - torsion coupling terms, was identified. After performing a factorial design analysis with the mentioned parameters, it was possible to calibrate a classical beam stiffness matrix through non-linear regression, in order to incorporate the information carried by a solid cable model.

The results obtained with the metaelement model were compared with those from Costello's analytical solution and FEM with solid elements for cables under tension, torsion, or bending. The metaelement showed substantially better agreement than the analytical model comparing the results obtained using solid elements. Based on the lower coefficient of determination attained for the coupling terms, the metaelement was found to yield larger deviations for coupling stiffnesses. The analytical model performed poorly under low helix angles, which is probably its most important weakness, as expected from previous reports. However, the deviations showed here between FEM and Costello's model were larger than those previously reported by Ghoreishi et al. (2007). Even though both studies used the same cable geometry (1×7), Ghoreishi considered isotropic materials and simplified contact conditions, which yielded lower deviations. Therefore, the metaelement presented here allows the modeling of very long cables, combining the accuracy of solid elements with the practical implementation of closed form solutions.

5. ACKNOWLEDGEMENTS

The authors would like to acknowledge the support of CNPQ and Propesq.

6. REFERENCES

Abaqus2013 Simulia Academic, 2013. Dassault SystémesAmericas Corp. Waltham, Massachusetts, USA.

Adanur, S., Ayman, S.M., Shinozuka, M. and Gumusel, L., 2011. "A comparative study on static and dynamic responses of FRP composite and steel suspension bridges". *Journal of Reinforced Plastics and Composites*, Vol. 30, No. 15, pp. 1265-1279.

Ali, A.H., Mohamed, H.M., Elsafty, A. and Benmokrane, B., 2015. "Long-term durability testing of tokyo rope carbon cables". *In International Conference of Composite Materials, ICCM20*, Copenhagen, Denmark.

Botker, S. and Johannessen, T.B., 2002. "Composite Risers and Tethers: The Future for Deep Water TLPs". In *OTC 14176 - Offshore Technology Conference*. Houston, USA.

Cai, H. and Aref, A.J., 2015. "On the design and optimization of hybrid carbon fiber reinforced polymer-steel cable system for cable-stayed bridges". *Composites: Part B*, Vol. 68, pp. 146-152.

Cardou, A. and Jolicoeur, C., 1997. "Mechanical models of helical strands". *Applied Mechanical Review*, Vol. 50, No. 1, pp. 1-14.

Chamis, C.C., 1989. "Mechanics of Composite Materials: Past, Present, and Future". *Journal of Composites Technology & Research*, Vol. 11, No. 1, pp.3-14.

Chen, Y., Meng, F. and Gong, X., 2017. "Study on performance of bended spiral strand with interwire frictional contact". *International Journal of Mechanical Sciences*, Vol. 128-129, pp. 499-511.

Costello, G.A., 1990. *Theory of Wire Rope*. Springer-Verlag, New York, 1st edition.

Ghoreishi, S.R., Messager, T., Cartraud, P., Davies, P., 2007. "Validity and limitations of linear analytical models for steel wire strands under axial loading, using a 3D FE model". *International Journal of Mechanical Sciences*, Vol. 12, pp. 1251-1261.

Jolicoeur, C., Cardou, A., 1996. "Semicontinuous Mathematical Model for Bending of Multilayered Wire Strands". *Journal of Engineering Mechanics*, Vol. 122, No. 7, pp. 643-650.

Kaddour, A.S., Hinton, M.J., 2004. "Instructions to Contributors of the Second World-Wide Failure Exercise". *WWFE-II: Part A*.

Liu, Y., 2016. "Advantages of using CFRP cables in orthogonally loaded cable structures". *Materials Science*, Vol. 3, No. 3, pp. 862-880.

Luz, F. F., Menezes, E. A. W., Silva, L. V., Cimini, C. A., Amico, S. C., 2018. "Strength analysis of composite cables". *Latin American Journal of Solids and Structures*, Vol. 15, No 4, pp. 1-9.

MATLAB R.version 8.0.0.783 (R2012b), 2012. The MathWorks Inc., Natick, Massachusetts.

Meier, U., 2012. "Carbon Fiber Reinforced Polymer Cables: Why? Why Not? What if?" *Arabian Journal for Science Engineering*, Vol. 37, pp. 399-411.

Menezes, E.A.W., Silva, L.V., Marczak, R.J., Amico, S.C., 2017. "Numerical model updating applied to the simulation of carbon fiber–reinforced polymer cables under bending and tensile stress". *Journal of Strain Analysis for Engineering Design*, Vol. 52, No. 6, pp. 356-364.

Odru, P., and Geffroy, R.L., 2002. "Carbon fiber tethers key for ultra-deepwater production". *Offshore*, Vol. 62.

Schön, J., 2004. "Coefficient of friction and wear of a carbon fiber epoxy matrix composite". *Wear*, Vol. 257, pp. 395-407.

Tauchert, T.R., 1974. *Energy Principles in Structural Mechanics*. McGraw-Hill.

Xie, X., Li, X. and Shen, Y., 2014. "Static and Dynamic Characteristics of a Long-Span Cable-Stayed Bridge with CFRP Cables". *Materials*, Vol. 7, pp. 4854-4877.

7. RESPONSIBILITY NOTICE

The authors are the only responsible for the printed material included in this paper.